Desalination and Water Treatment
www.deswater.com

doi: 10.5004/dwt.2020.25426

185 (2020) 247–261
May

Hydrothermal synthesis of $CaTiO_3$ cuboid-like nanoparticles starting from metatitanic acid and calcium hydroxide and their adsorption performance for Cd(II), Pb(II), Ni(II), and Co(II) cations

Qin Zhou, Aili Wang*, Hengbo Yin*

Faculty of Chemistry and Chemical Engineering, Jiangsu University, Zhenjiang 212013, China, Tel. +86-(0)511-88787591; Fax: +86-(0)511-88791800; email: alwang@ujs.edu.cn (A. Wang), yin@ujs.edu.cn (H. Yin), z.qinemily@foxmail.com (Q. Zhou)

Received 14 June 2019; Accepted 30 December 2019

ABSTRACT

Calcium titanate ($CaTiO_3$) cuboid-like nanoparticles with the average widths and lengths of 101–184 and 203–329 nm were hydrothermally synthesized using metatitanic acid and calcium hydroxide as starting materials at 120°C–180°C. Metatitanic acid is an intermediate in the commercial TiO_2 pigment production by the sulfuric acid method. High hydrothermal temperature favored the formation of small-sized $CaTiO_3$ cuboid-like nanoparticles. When the $CaTiO_3$ cuboid-like nanoparticles were used as the absorbents for the removal of heavy metallic cations from aqueous solution, the Langmuir adsorption isotherms showed that the maximum adsorption capacities of the $CaTiO_3$ cuboid-like nanoparticles for Pb(II), Cd(II), Ni(II), and Co(II) cations were 237.0, 74.7, 60.8 and 61.2 mg g^{-1}, respectively. The thermodynamic analysis revealed that the adsorption process of these metallic cations was spontaneous and endothermic.

Keywords: $CaTiO_3$ cuboid-like nanoparticles; Hydrothermal method; Adsorption kinetics; Adsorption isotherm; Thermodynamics; Heavy metals

1. Introduction

Calcium titanate with the Perovskite structure can be used as the dielectric material [1–3], sensor [4], alkaline catalyst in the transesterification of waste cooking oil into biodiesel [5], absorbent for the removal of heavy metallic cations [6], and photocatalyst in the degradation of dyes [6,7], oxidation of As(III) to As(V) [8], and reduction of CO_2 with water to CO under UV light irradiation [9]. Calcium titanate can also be used as the biomaterial for the Schwann cell growth in peripheral nerve regeneration and bone-bonding on bone repair materials [10–13].

Calcium titanate powders with the particle sizes ranging from dozens of nanometers to several micrometers could be synthesized by the conventional solid-state reaction technique at high reaction temperatures of 400°C–1300°C using $CaCO_3/TiO_2$ [1,9], $CaCO_3$/titanium (IV) isopropoxide [14], $CaCl_2/TiO_2$ [15], $Ca(NO_3)_2$/titanium *n*-butoxide [7], and $Ca(NO_3)_2{\cdot}4H_2O/TiO_2$ (P25) [4] as starting materials.

For the synthesis of $CaTiO_3$ nanoparticles, the spray-pyrolysis method was used starting from $Ca(NO_3)_2$/titanium (IV) isopropoxide at 750°C–850°C [16]. The hydrothermal method was also used to synthesize $CaTiO_3$ nanoparticles with the use of $Ca(NO_3)_2{\cdot}4H_2O/TiCl_4$ (titanium isopropoxide or titanium *n*-butoxide) and $CaCl_2$/anatase TiO_2 as starting materials at 110°C–180°C [8,17]. Compared with the solid-state reaction and spray-pyrolysis methods, the hydrothermal method can be carried out at mild reaction temperature. However, to the best of our knowledge, the synthesis of $CaTiO_3$ nanoparticles by the hydrothermal method using $Ca(OH)_2$ and metatitanic acid (an intermediate in TiO_2 pigment production) has not been reported until now.

* Corresponding authors.

With the rapid development in economy and industry, natural water pollution has caused that one-fifth of the world's population has no access to safe water [18]. Heavy metal pollution, such as vanadium, nickel, cadmium, lead, chromium, silver, and mercury, has a great impact on the metabolism of human beings [19–23]. Nowadays, numerous methods have been used for the removal of heavy metallic cations from polluted water, such as adsorption [24,25], microbial degradation [26], ion exchange [27], membrane separation, and coagulation [28]. Among these methods, the adsorption method is known to be most suitable for the removal of heavy metals at a lower cost. The $CaTiO_3$ powders synthesized by the solid-state reaction method exhibited good adsorption capacities for heavy metallic cations [29–31]. It was reported that the adsorption capacities of porous $CaTiO_3$ powders for Pb(II), Cd(II), Zn(II), Cu(II), and Ni(II) cations in aqueous solutions were 141.8–230.2, 18.0–32.5, 24.4–66.0, 88.1, and 23.9 mg g^{-1}, respectively [29–31]. However, the adsorption capacities, kinetics, and thermodynamics of heavy metallic cations on $CaTiO_3$ nanoparticles synthesized at a lower reaction temperature (<200°C) have rarely been investigated.

In this work, $CaTiO_3$ cuboid-like nanoparticles were synthesized by the hydrothermal method using metatitanic acid and calcium hydroxide as raw materials at different reaction temperatures. The evolution process of $CaTiO_3$ nanoparticles was discussed. The adsorption kinetics, isotherms, and thermodynamics of Pb(II), Cd(II), Ni(II), and Co(II) cations on the $CaTiO_3$ cuboid-like nanoparticles were simulated.

2. Experimental setup

2.1. Materials

Metatitanic acid (36 wt.% TiO_2) was supplied by the Jiangsu Taibai Group Co. Ltd., China. Sodium hydroxide, lead(II) nitrate, cobalt(II) nitrate, nickel(II) chloride, and cadmium(II) nitrate were of analytical grade and were purchased from Shanghai Chemical Reagent Co. Ltd., China.

2.2. Preparation of calcium titanate nanoparticles

Metatitanic acid (based on TiO_2, 20 g) was dispersed in 450 mL deionized water in a 1 L plastic beak under magnetic stirring for 15 min. A sodium hydroxide (2.5 mol L^{-1}) aqueous solution was added slowly into the metatitanic acid suspension to adjust the pH value of 7. 18.8 g (0.25 mol) of calcium hydroxide was dissolved in 50 mL deionized water and added into the metatitanic acid suspension with a Ca/Ti mole ratio of 1:1 under stirring for 2 h. The mixture was transferred into an autoclaved at 120°C–180°C for 4–16 h. After the hydrothermal reaction, the precipitate was filtrated and washed with deionized water until the pH value of filtrate was decreased to 7. The precipitate sample was dried at 100°C in an electric oven overnight and then kept in a desiccator.

2.3. Adsorption experiments

A given amount of lead(II) nitrate, cobalt(II) nitrate, nickel(II) chloride, and cadmium(II) nitrate were dissolved in 250 mL deionized water at 25°C, respectively. Under magnetic stirring, 1.0 g of $CaTiO_3$ was added into these metallic cation aqueous solutions. The concentrations of the metallic cations in the solutions were determined by the atomic absorption spectrometry at different adsorption time periods by taking 3.0 mL of an aqueous suspension. The aqueous suspension was filtrated before analysis.

2.4. Characterization

The X-ray powder diffraction (XRD) patterns of the $CaTiO_3$ samples were determined on a D8 super speed X-ray diffractometer in a range of 10°–90° (2θ) with Cu Kα radiation at λ = 1.5406 Å. The morphologies of the $CaTiO_3$ samples were observed on a scanning electron microscope (SEM) (HiTachi S-4800, Hitachi, Japan). The concentrations of Cd(II), Pb(II), Ni(II), and Co(II) in aqueous solutions were analyzed by the atomic absorption spectrometry (TAS-986). The elements of the $CaTiO_3$ sample were analyzed by the energy-dispersion X-ray spectroscopy (EDX) (JSM-6010 PLUS/LA, JEOL, Japan, 15 kV). The point of zero charges for the $CaTiO_3$ sample was measured on a NanoBrook 90PlusPALS, Brookhaven, USA. The band gaps of the $CaTiO_3$ sample was determined by the UV-visible diffuse reflectance spectroscopy.

3. Results and discussion

3.1. Chemical structure and morphology of $CaTiO_3$ sample

The XRD patterns of the $CaTiO_3$ samples synthesized at different temperatures are shown in Fig. 1. When the hydrothermal reaction was carried out at 120°C and 140°C for 4–8 h, the samples contained two phases of anatase TiO_2 (JCPDS 21-1272) and $CaTiO_3$ (JCPDS 78–1013). When the reaction time period was prolonged to 12 h or longer, the samples were mainly composed of $CaTiO_3$ phase.

When the hydrothermal reaction was carried out at 160°C and 180°C for 8 h or longer, the as-synthesized samples were mainly composed of $CaTiO_3$ phase. The results revealed that high reaction temperature and long reaction time favored the evolution of $CaTiO_3$ phase through the reaction between anatase TiO_2 and $Ca(OH)_2$.

The SEM images of the $CaTiO_3$ samples synthesized at different reaction temperatures are shown in Fig. 2. When the hydrothermal reaction was carried out at 120°C for 4 h, a large number of nanoparticles with the average particle size of 35 nm were formed, which should be ascribed to anatase TiO_2 nanoparticles (Fig. 2a1). An only a small amount of $CaTiO_3$ cuboid-like nanoparticles was observed in this sample. When the reaction time periods were 8–16 h, the $CaTiO_3$ cuboid-like nanoparticles were dominantly formed with the average widths and lengths of 148.7–184.1 and 236.5–329.5 nm, respectively (Figs. 2a2–a4, Table 1).

At the reaction temperature of 140°C, the $CaTiO_3$ cuboid-like nanoparticles were formed at a shorter reaction time of 4 h. When the reaction time periods were 8–16 h, the $CaTiO_3$ cuboid-like nanoparticles with the average widths and lengths of 137.1–162.6 and 240.2–292.1 nm were dominantly formed (Figs. 2b2–b4, Table 1).

When the reaction temperatures were raised to 160°C and 180°C, the $CaTiO_3$ cuboid-like nanoparticles were formed even at a shorter reaction time period of 4 h. The average

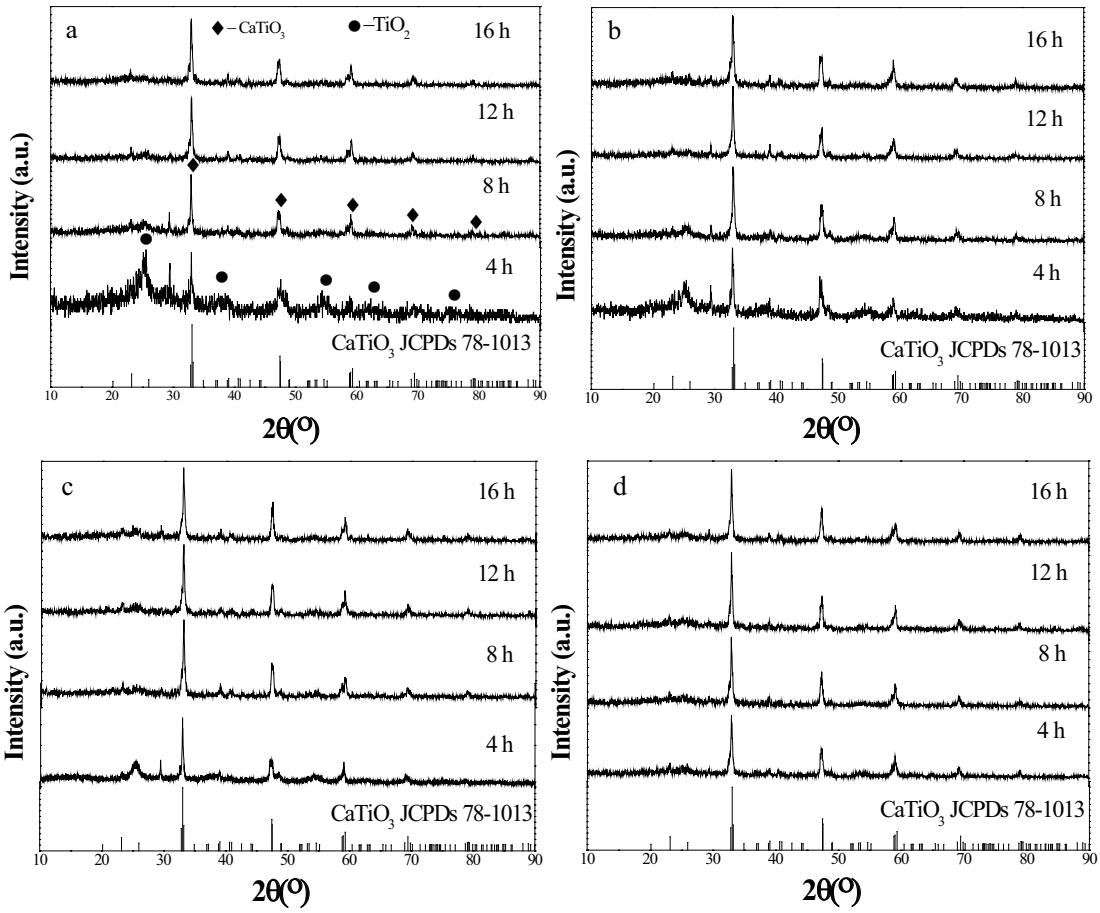

Fig. 1. X-ray diffraction patterns of the $CaTiO_3$ samples hydrothermally synthesized at different reaction temperatures of (a) 120°C, (b) 140°C, (c) 160°C, and (d) 180°C for 4–16 h.

widths and lengths of the as-synthesized $CaTiO_3$ cuboid-like nanoparticles were 121.1–144.0, 221.0–251.7; 101.3–126.7, and 203.5–233.4 nm, respectively (Figs. 2c and 2d).

It was found that high reaction temperature favored the formation of small-sized $CaTiO_3$ cuboid-like nanoparticles. However, their specific surface areas decreased upon increasing the reaction temperature or prolonging the reaction time period (Table 1). It could be explained as that at a higher reaction temperature, more $CaTiO_3$ crystal nucleus could be rapidly formed, resulting in the formation of small-sized $CaTiO_3$ cuboid-like nanoparticles. However, the crystallinity of the $CaTiO_3$ cuboid-like nanoparticles was improved at higher reaction temperature and a longer reaction time period, giving a lower specific surface area.

3.2. Elemental composition, point of zero charge, and band gap of $CaTiO_3$ cuboid-like nanoparticles

The elements of the $CaTiO_3$ cuboid-like nanoparticles hydrothermally synthesized at 160°C for 12 h were analyzed by the EDX technique. The EDX analysis showed that the elements of calcium, titanium, and oxygen were present in the as-synthesized sample. The atomic ratio of Ca^{2+} to Ti^{4+} in the $CaTiO_3$ sample was around 1:1 (Fig. 3), being close to that of pure $CaTiO_3$.

The point of zero charges of the $CaTiO_3$ cuboid-like nanoparticles hydrothermally synthesized at 160°C for 12 h is shown in Fig. 4. The point of zero charges of the $CaTiO_3$ sample was at the pH value of 2.9. The band gap of the $CaTiO_3$ sample was determined by the UV-visible diffuse reflectance spectroscopy (Fig. 5). The band gap of the $CaTiO_3$ sample was 3.68 eV.

3.3. Adsorption of heavy metallic cations

3.3.1. Adsorption of heavy metallic cations on $CaTiO_3$ cuboid-like nanoparticles

The $CaTiO_3$ cuboid-like nanoparticles hydrothermally synthesized at 160°C for 12 h were used as the adsorbents. The adsorption capacities of $CaTiO_3$ cuboid-like nanoparticles for Cd(II), Pb(II), Ni(II), and Co(II) metallic cations in aqueous solutions are shown in Fig. 6. When the $CaTiO_3$ dosages were in a range of 0.5–1.2 g, the adsorption capacities of the $CaTiO_3$ cuboid-like nanoparticles slightly decreased upon increasing the $CaTiO_3$ dosage. When the adsorption time period was 300 min, the adsorption capacities of the $CaTiO_3$ cuboid-like nanoparticles for Cd(II), Pb(II), Ni(II), and Co(II) metallic cations were around 28, 110, 32, and 33 mg g^{-1}, respectively.

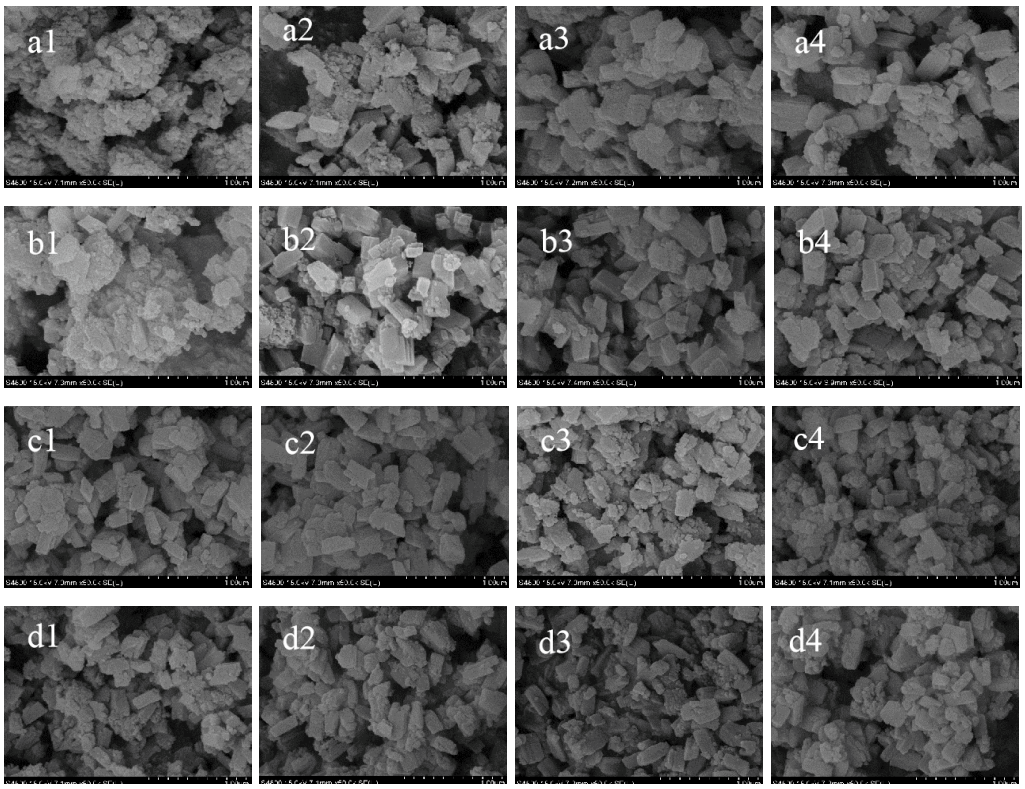

Fig. 2. SEM images of the $CaTiO_3$ samples hydrothermally synthesized at different hydrothermal reaction temperatures of (a1–a4) 120°C, (b1–b4) 140°C, (c1–c4) 160°C, and (d1–d4) 180°C for 4, 8, 12, and 16 h, respectively. The scale bar is 1 μm.

Table 1
Particle sizes and specific surface areas of the $CaTiO_3$ samples

Hydrothermal reaction temperatures (°C)	Reaction time periods (h)	Particle sizes of $CaTiO_3$ cuboid-like nanoparticles		Specific surface areas ($m^2\ g^{-1}$)
		Average widths (nm)	Average lengths (nm)	
120	4	100 35.0 (Particulates)	150	137
	8	148.7 35.0 (Particulates)	275.7	74
	12	156.8	236.5	38
	16	184.1	329.5	24
140	4	139.1 35.0 (Particulates)	273.0	101
	8	141.2	240.2	56
	12	137.1	292.1	28
	16	162.6	282.8	19
160	4	121.1	223.7	52
	8	144.0	247.7	38
	12	140.2	251.7	33
	16	125.5	221.0	23
180	4	126.0	233.4	51
	8	126.7	231.9	37
	12	101.3	203.5	28
	16	112.0	214.9	27

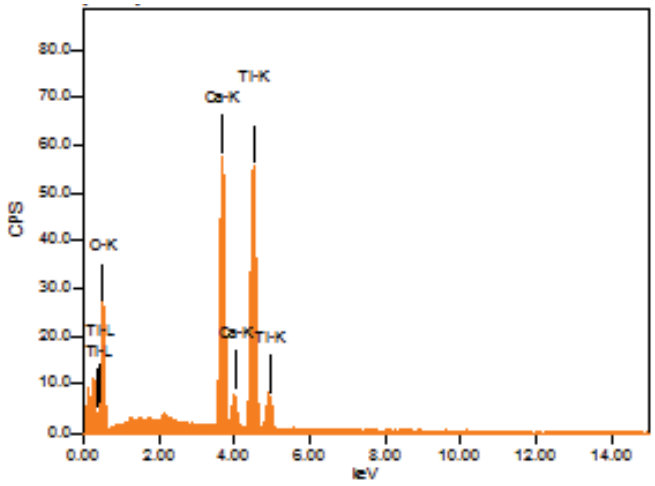

Fig. 3. EDX spectra of the $CaTiO_3$ cuboid-like nanoparticles hydrothermally synthesized at 160°C for 12 h.

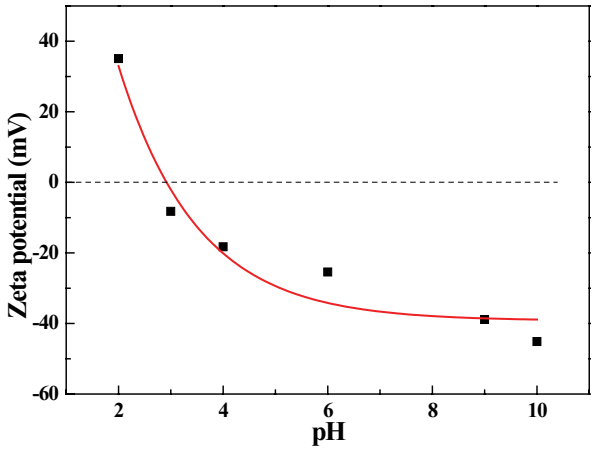

Fig. 4. pH_{pzc} plot of the $CaTiO_3$ cuboid-like nanoparticles hydrothermally synthesized at 160°C for 12 h.

The adsorption capacities of the $CaTiO_3$ cuboid-like nanoparticles for the metallic cations at different pH values are shown in Fig. 7. When the adsorption time period was 300 min, upon increasing the pH values from 3 to 8, the adsorption capacities of the $CaTiO_3$ cuboid-like nanoparticles for Cd(II), Pb(II), Ni(II) and Co(II) metallic cations increased from 22 to 37, 99 to 140, 23 to 33, and 31 to 37 mg g^{-1}, respectively. According to the point of zero charge analysis, it could be explained that the adsorption capacities of $CaTiO_3$ cuboid-like nanoparticles were affected by the surface charge property of $CaTiO_3$ cuboid-like nanoparticles. Pb(II) cation had a higher adsorption capacity than the other metallic cations. The reason may be due to that Pb(II) cation has a higher electrophilicity, exhibiting a higher adsorption ability on the negatively charged $CaTiO_3$ surface at a pH value of 7.

3.3.2. Adsorption kinetics

The adsorption kinetic experiments were carried out at 25°C by adding 1.0 g of $CaTiO_3$ cuboid-like nanoparticles

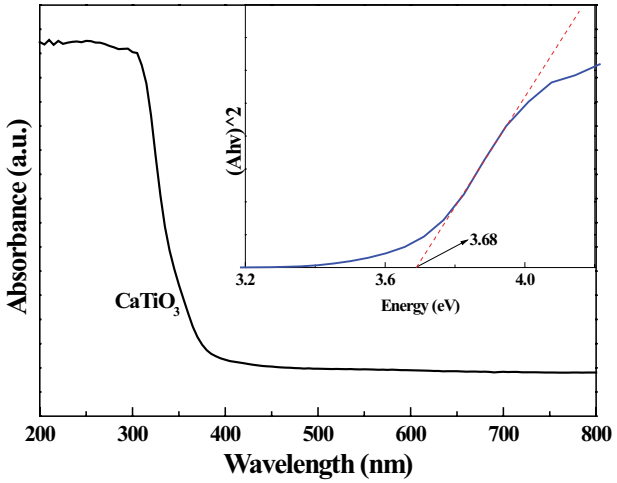

Fig. 5. UV-visible diffuse reflectance spectra of the $CaTiO_3$ cuboid-like nanoparticles hydrothermally synthesized at 160°C for 12 h.

hydrothermally synthesized at 160°C for 12 h into 250 mL of heavy metallic cation aqueous solutions under stirring. The concentrations of heavy metallic cations were analyzed at different adsorption time periods. The adsorption kinetics of heavy metallic cations on the $CaTiO_3$ nanoparticles are simulated by the pseudo-first-order Eq. (1), pseudo-second-order Eq. (2), and Weber–Morris Eq. (3) adsorption kinetic equations [32–35].

$$q_t = q_e\left(1-\exp\left(-k_1 t\right)\right) \tag{1}$$

$$\frac{t}{q_t} = \frac{1}{\left(k_2 q_e^2\right)} - \frac{t}{q_e} \tag{2}$$

$$q_t = k_{id} t^{0.5} + C \tag{3}$$

where q_t and q_e (mg g^{-1}) are the adsorption capacities of $CaTiO_3$ cuboid-like nanoparticles for heavy metallic cation at time t and equilibrium, respectively. k_1 (min^{-1}), k_2 (g mg^{-1} min^{-1}), and k_{id} (mg g^{-1} $min^{-0.5}$) are the rate constants of the pseudo-first-order, pseudo-second-order, and Weber–Morris equations. C (mg g^{-1}) is the thickness of the boundary layer. C_0 and C_e are the initial and equilibrium concentrations of metallic cations (mg L^{-1}).

The adsorption amount of the metallic cations, Cd(II), Pb(II), Ni(II), and Co(II) on the $CaTiO_3$ cuboid-like nanoparticles steeply increased at the initial 30 min (Figs. 8a–d), probably due to the high concentration gradient of heavy metal cation between bulk solution and $CaTiO_3$ nanoparticle surface as well as the expose of more adsorption sites at the $CaTiO_3$ cuboid-like nanoparticle surface.

Adsorption kinetic simulation of metallic cations on $CaTiO_3$ cuboid-like nanoparticles is shown in Fig. 8. The Kinetic parameters and correlation coefficients simulated according to the three adsorption kinetic models are listed in Table 2. By comparing the values of a correlation coefficient, R^2, it was found that the pseudo-second-order

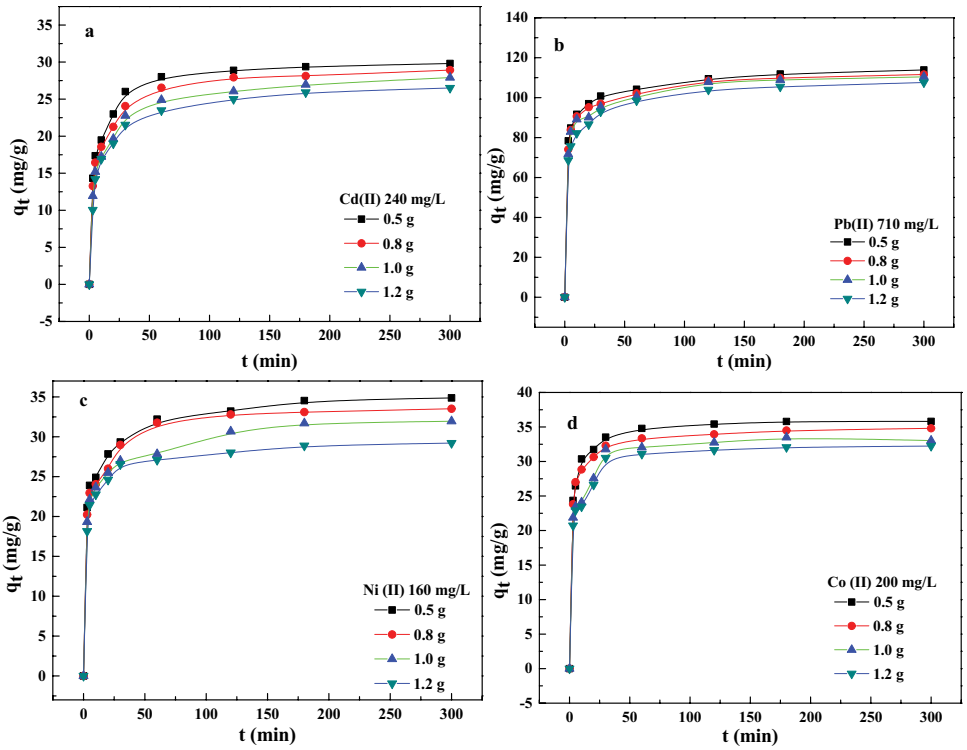

Fig. 6. Adsorption capacities of $CaTiO_3$ cuboid-like nanoparticles for Cd(II), Pb(II), Ni(II) and Co(II) metallic cations in aqueous solutions at 25°C and pH value of 7 with different $CaTiO_3$ dosages. The $CaTiO_3$ cuboid-like nanoparticles were hydrothermally synthesized at 160°C for 12 h.

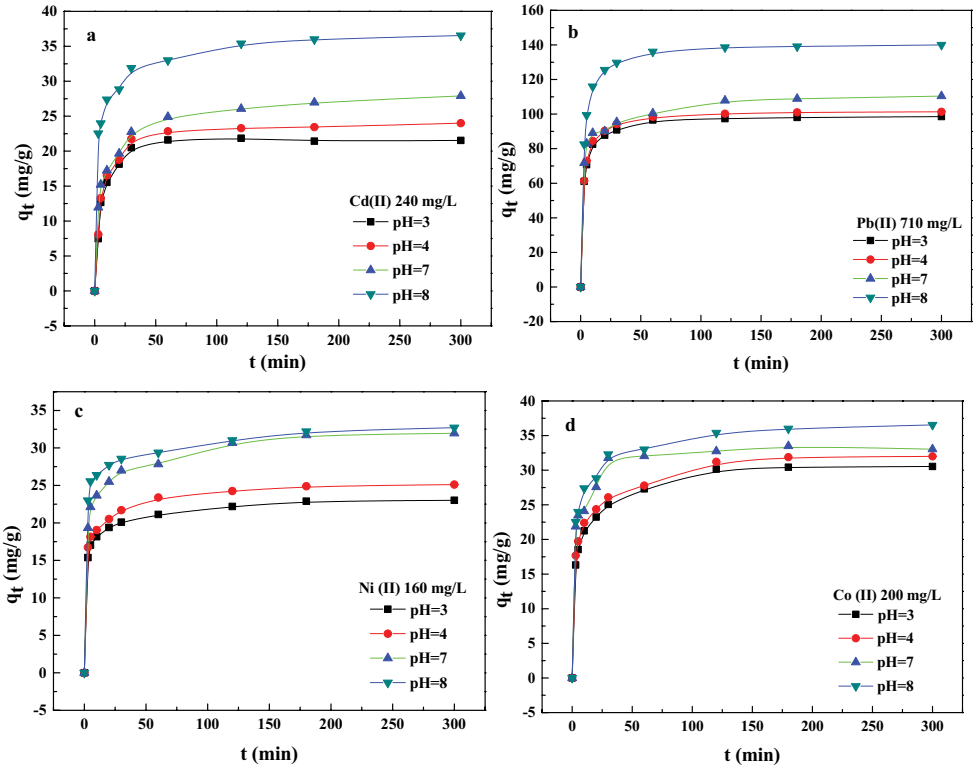

Fig. 7. Adsorption capacities of the $CaTiO_3$ cuboid-like nanoparticles for (a) Cd(II), (b) Pb(II), (c) Ni(II), and (d) Co(II) metallic cations in aqueous solutions at different pH values and 25°C. The $CaTiO_3$ cuboid-like nanoparticles were hydrothermally synthesized at 160°C for 12 h.

Table 2
Kinetic parameters of the adsorption of Cd(II), Pb(II), Ni(II), and Co(II) cations on $CaTiO_3$ cuboid-like nanoparticles under different initial concentrations at 25°C and pH value of 7

Metallic cations	C_0 (mg L^{-1})	Pseudo-first-order kinetic model			Pseudo-second-order kinetic model			Weber–Morris kinetic model		
		k_1 (min^{-1})	q_e (mg g^{-1})	R^2	k_2 (g mg^{-1} min^{-1})	q_e (mg g^{-1})	R^2	C (mg g^{-1})	k_{id} (mg g^{-1} $min^{-0.5}$)	R^2
Cd(II)	240	0.1519	25.0	0.9141	0.0062	28.1	0.9990	10.7848	1.2746	0.7541
	280	0.1816	29.3	0.9265	0.0066	32.5	0.9993	13.6997	1.4091	0.5995
	320	0.2183	32.4	0.9208	0.0066	36.0	0.9994	16.1042	1.5015	0.5618
	360	0.3589	36.8	0.9631	0.0114	39.5	0.9999	21.8127	1.4101	0.3862
Pb(II)	710	0.3701	100.9	0.9642	0.0030	111.0	0.9996	58.8928	4.0281	0.4220
	760	0.3977	107.5	0.9352	0.0028	118.5	0.9996	63.6848	4.2454	0.4121
	810	0.3974	113.0	0.9420	0.0030	123.6	0.9998	67.2932	4.4083	0.4008
	860	0.3935	121.6	0.9834	0.0048	127.7	0.9999	75.6042	4.2482	0.3101
Ni(II)	160	0.3106	28.7	0.9218	0.0077	32.2	0.9992	15.7000	1.2444	0.5009
	200	0.3322	35.7	0.9699	0.0098	38.4	0.9996	20.8076	1.3815	0.3855
	240	0.3665	40.2	0.9737	0.0129	43.3	0.9999	24.1678	1.4966	0.3587
	280	0.4884	43.4	0.9600	0.0077	47.1	0.9997	27.2728	1.5629	0.3325
Co(II)	200	0.3077	31.1	0.9182	0.0142	33.4	0.9997	17.5648	1.2687	0.4332
	240	0.3766	35.0	0.9578	0.0090	38.2	0.9995	20.8184	1.3514	0.3875
	280	0.3976	39.3	0.9673	0.0094	42.4	0.9996	23.8194	1.4646	0.3628
	320	0.446	42.1	0.9901	0.0133	44.1	0.9997	26.9844	1.3946	0.2689

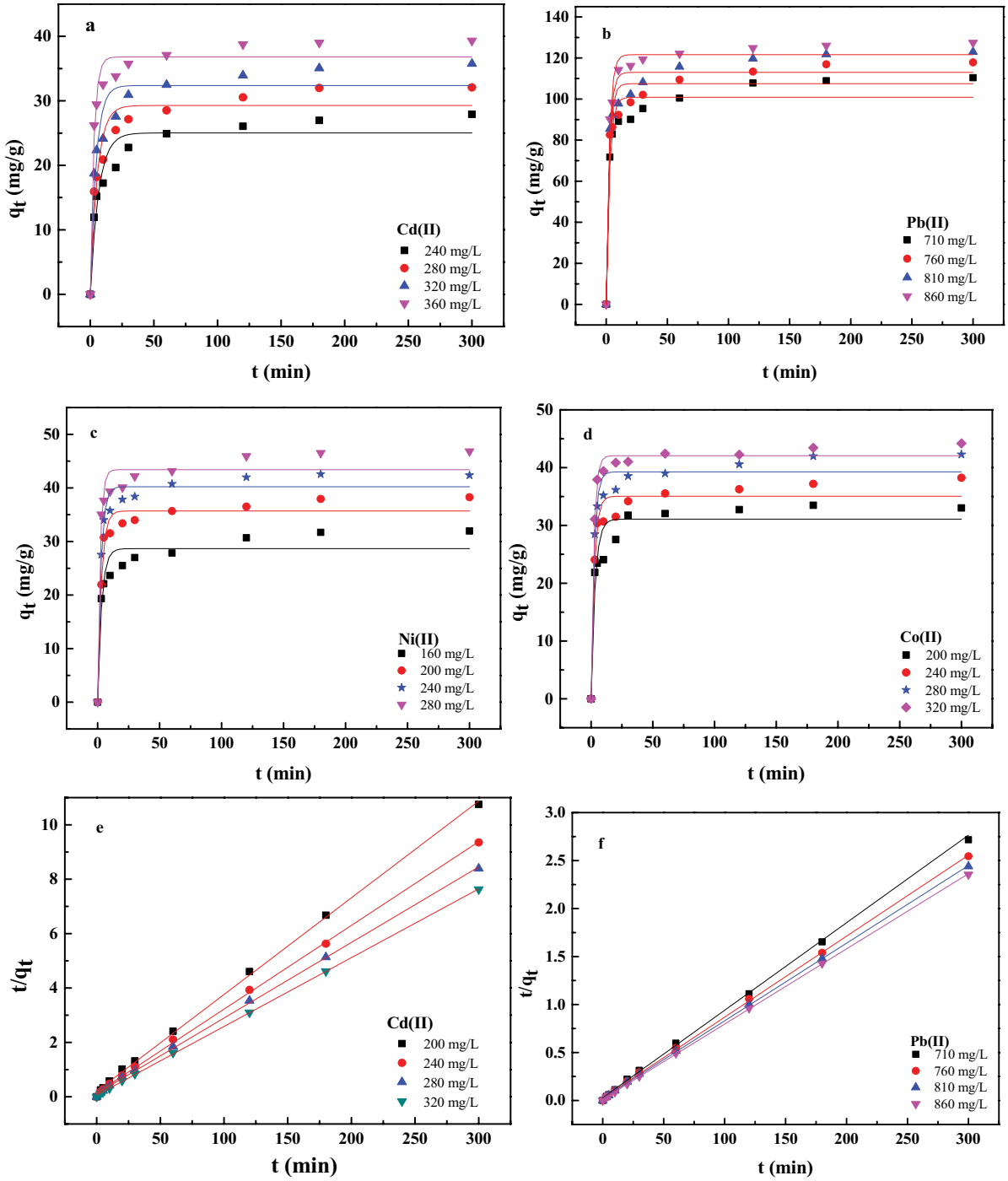

Fig. 8. *Continued*

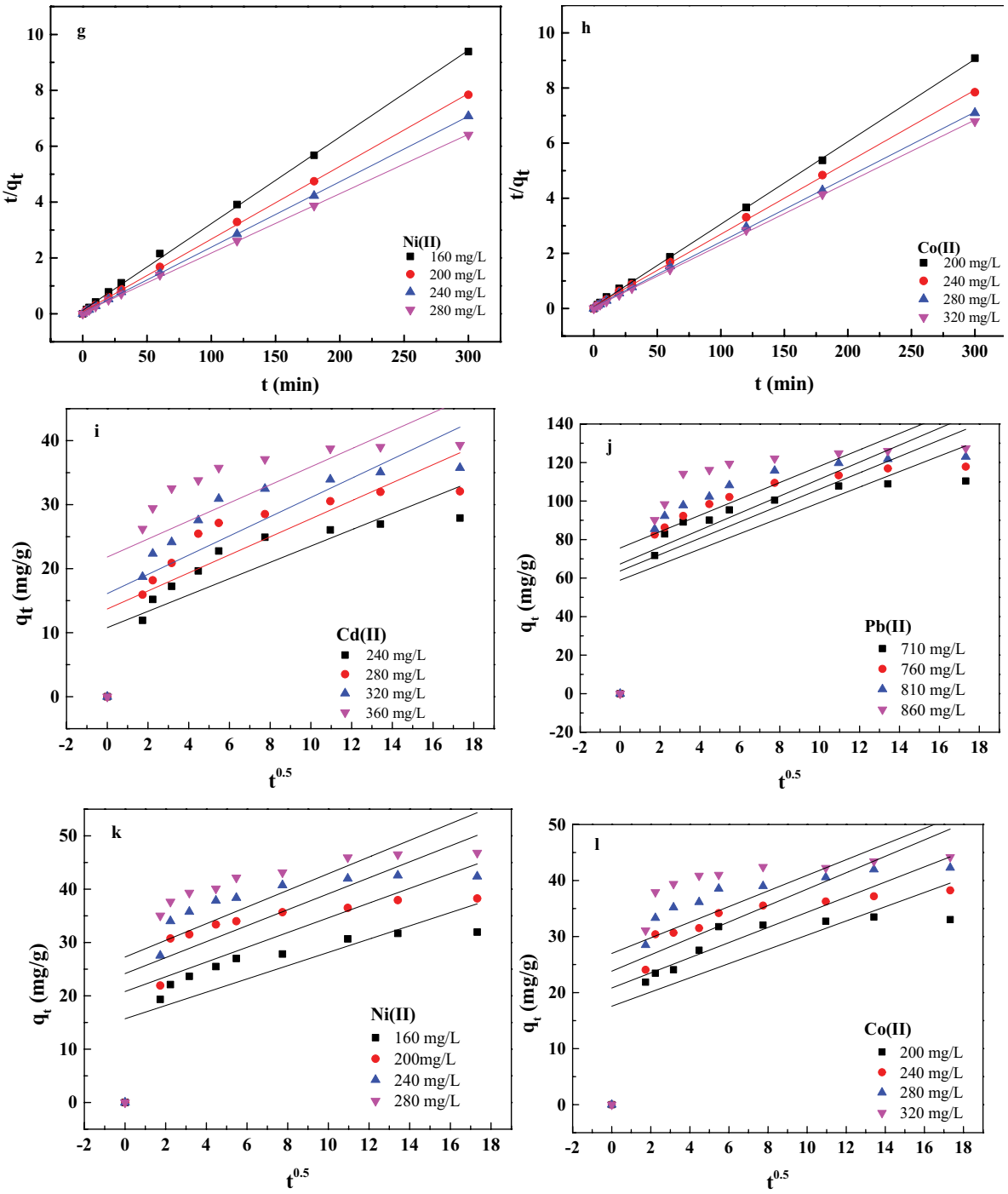

Fig. 8. Adsorption kinetic simulation of the metallic cations on $CaTiO_3$ cuboid-like nanoparticles at 25°C and pH value of 7. Solid lines represent the fitting results using (a–d) the pseudo-first-order, (e–h) pseudo-second-order, and (i–l) Weber–Morris adsorption models.

adsorption kinetic model well fitted the experimental data. The simulation of adsorption kinetics revealed that the adsorption kinetics of these cations on the $CaTiO_3$ surfaces was neither affected by the diffusion of the metallic cation from the solution to $CaTiO_3$ surface nor by the intraparticle diffusion. The adsorption kinetics could be affected by the interaction between the metallic cations and the active sites at the $CaTiO_3$ surfaces.

3.3.3. Adsorption isotherms

The Langmuir, Freundlich, and Dubinin–Radushkevich adsorption isotherm models were used to fit the adsorption isotherms of the metallic cations on the $CaTiO_3$ cuboid-like nanoparticles [32–36]. The linear form of the Langmuir isotherm is expressed as Eq. (4).

$$\frac{C_e}{q_e} = \frac{1}{\left(K_L q_{\max}\right)} + \frac{C_e}{q_{\max}} \tag{4}$$

where $q_{\max}$ (mg g^{-1}) is the maximum adsorption capacity. q_e (mg g^{-1}) is the adsorption capacity at equilibrium, and C_e (mg L^{-1}) is the concentration at equilibrium. K_L (L mg^{-1}) is the Langmuir constant.

The linear form of the Freundlich adsorption isotherm is expressed as Eq. (5).

$$\ln q_e = \ln K_F + \left(\frac{1}{n}\right)\ln C_e \tag{5}$$

where K_F (mg g^{-1} (mg $L^{-1})^{-1/n}$) is the Freundlich constant. q_e (mg g^{-1}) is the equilibrium adsorption capacity. C_e (mg L^{-1}) is the equilibrium concentration, and $1/n$ refers to the intensity of adsorption.

The linear form of the Dubinin–Radushkevich adsorption isotherm is expressed as Eq. (6).

$$\ln q_e = \ln q_{\max} - B_D \varepsilon^2 \tag{6}$$

where q_e (mg g^{-1}) is the adsorption amount at equilibrium. B_D (mol^2 J^{-2}) is the activity factor related to the mean energy of adsorption. ε is the Polanyi potential and can be calculated by Eq. (7).

$$\varepsilon = RT \ln\left(1 + \frac{1}{C_e}\right) \tag{7}$$

The mean adsorption free energy E (J mol^{-1}) could be calculated according to Eq. (8).

$$E = \left(2B_D\right)^{-1/2} \tag{8}$$

Simulation of experimental data using the Langmuir, Freundlich, and Dubinin–Radushkevich isotherm models are shown in Fig. 9. The values of K_L and $q_{\max}$ were obtained according to the simulated straight lines using the Langmuir isotherm model (Figs. 9a–d). While using the Freundlich

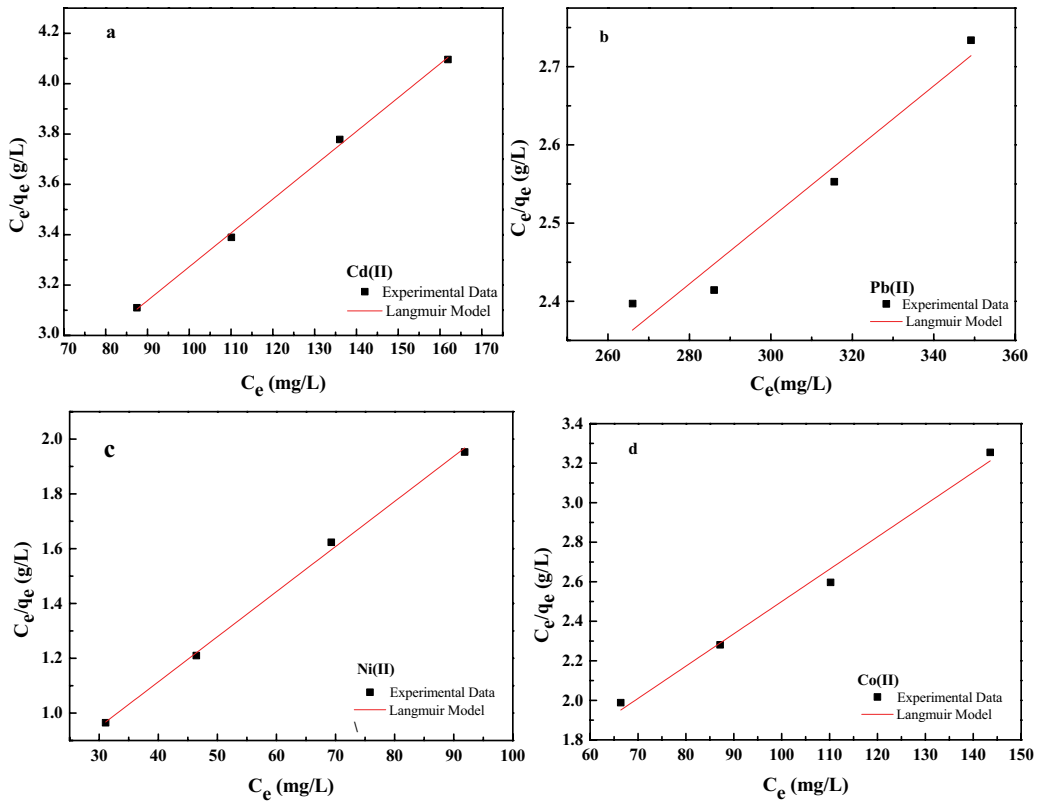

Fig. 9. *Continued*

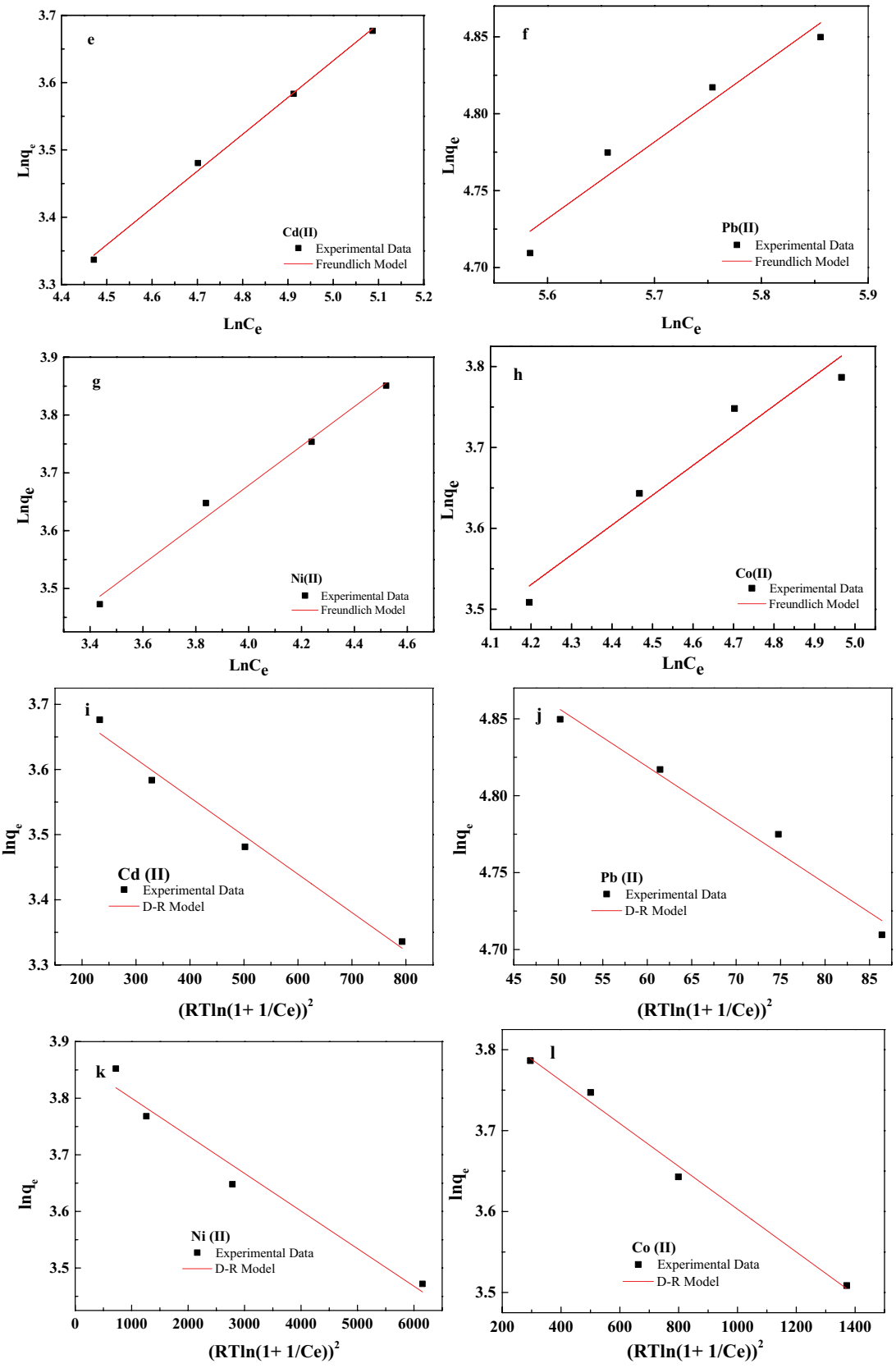

Fig. 9. The Langmuir (a–d), Freundlich (e–h), and Dubinin–Radushkevich (i–l) adsorption isotherms for metallic cation adsorption at 25°C and pH value of 7.

isotherm model, the values of K_F and $1/n$ were obtained from the intercepts and the slopes of the straight lines (Figs. 9e–h). The Dubinin–Radushkevich adsorption parameters, $\ln q_{max}$ and B_D, were calculated according to the intercept and slope of the plot of $\ln q_e$ vs $(RT\ln(1 + 1/C_e))^2$ (Figs. 9i–l). The data of the simulated parameters using the Langmuir, Freundlich, and Dubinin–Radushkevich models are listed in Table 3.

Considering that the values of the correlation coefficient, R^2, obtained using the Langmuir isotherm were larger than those using the Freundlich isotherm, it was suggested that the adsorption was probably a monolayer surface adsorption of the metal cations at the surfaces of $CaTiO_3$ cuboid-like nanoparticles. According to the estimation by the Langmuir adsorption isotherm, the maximum adsorption capacities of $CaTiO_3$ cuboid-like nanoparticles for the Cd(II), Pb(II), Ni(II), and Co(II) cations were 74.7, 237.0, 60.8 and 61.2 mg g^{-1}, respectively. It was reported that the adsorption capacities of porous $CaTiO_3$ powders synthesized by the solid-state reaction method for the Cd(II), Pb(II), and Ni(II) cations from aqueous solutions were 18.0–32.5, 141.8–230.2, and 23.9 mg g^{-1}, respectively [29–31]. The as-synthesized $CaTiO_3$ cuboid-like nanoparticles exhibited higher adsorption capacities for these metallic cations than the porous $CaTiO_3$ powders.

According to the Dubinin–Radushkevich isotherms and the calculation method reported in the references [35,36], the mean adsorption free energies (E) of Cd(II), Pb(II), Ni(II), and Co(II) cations on the $CaTiO_3$ cuboid-like nanoparticles were 0.03, 0.01, 0.09, and 0.04 kJ mol^{-1}, respectively. It is suggested that the adsorption process is physical adsorption when the E value is less than 8 kJ mol^{-1} [35,36]. Considering that the mean adsorption free energies (E) of these cations were obviously less than 8 kJ mol^{-1}, their adsorption processes were of physical adsorption nature.

3.3.4. Adsorption thermodynamics

To assess the adsorption thermodynamics of the Cd(II), Pb(II), Ni(II), and Co(II) cations on the $CaTiO_3$ cuboid-like nanoparticles, the adsorption experiments were conducted at the pH value of 7 and different temperatures of 298, 313, and 328 K under different concentrations. The standard Gibb's free energy change, $\Delta G°$ (J mol^{-1}), can be obtained according to the following equation:

$$\Delta G° = -RT\ \ln K_c \tag{9}$$

where R (8.314 J K^{-1} mol^{-1}) is the universal gas constant, T (K) is the temperature of metallic cation aqueous solution. K_c (L mol^{-1}) is the Langmuir constant [37–39].

Table 3
Parameters of the Langmuir, Freundlich, and Dubinin–Radushkevich isotherms and the correlation coefficients for the adsorption of Cd(II), Pb(II), Ni(II), and Co(II) cations on $CaTiO_3$ cuboid-like nanoparticles at 25°C and pH value of 7

Metallic cations	Models	Equations	R^2	Parameters	Estimated values
Cd(II)	Langmuir	$q_e = q_{max}K_LC_e/(1 + K_LC_e)$	0.9975	q_{max}	74.7
				K_L	0.0070
	Freundlich	$q_e = K_FC_e^{1/n}$	0.9956	K_F	2.4547
				$1/n$	0.5469
	Dubinin–Radushkevich	$\ln q_e = \ln q_{max} - B_D\varepsilon^2$	0.9763	q_{max}	44.3752
				B_D	5.8904E-4
Pb(II)	Langmuir	$q_e = q_{max}K_LC_e/(1 + K_LC_e)$	0.9387	q_{max}	236.96
				K_L	0.0034
	Freundlich	$q_e = K_FC_e^{1/n}$	0.9205	K_F	6.9545
				$1/n$	0.4986
	Dubinin–Radushkevich	$\ln q_e = \ln q_{max} - B_D\varepsilon^2$	0.9615	q_{max}	155.4805
				B_D	0.00379
Ni(II)	Langmuir	$q_e = q_{max}K_LC_e/(1 + K_LC_e)$	0.9972	q_{max}	60.8
				K_L	0.0362
	Freundlich	$q_e = K_FC_e^{1/n}$	0.9840	K_F	2.3157
				$1/n$	0.3407
	Dubinin–Radushkevich	$\ln q_e = \ln q_{max} - B_D\varepsilon^2$	0.9512	q_{max}	47.7687
				B_D	6.6414E-5
Co(II)	Langmuir	$q_e = q_{max}K_LC_e/(1 + K_LC_e)$	0.9861	q_{max}	61.2
				K_L	0.0189
	Freundlich	$q_e = K_FC_e^{1/n}$	0.9238	K_F	7.2573
				$1/n$	0.3687
	Dubinin–Radushkevich	$\ln q_e = \ln q_{max} - B_D\varepsilon^2$	0.9888	q_{max}	47.8208
				B_D	2.6451E-4

Based on the relationship of q_e (mg g^{-1}) vs. C_e (mol L^{-1}) at different temperatures (Fig. 10), the values of K_c were simulated. And then the values of $\Delta G°$ could be calculated by Eq. (9). The data of K_c and $\Delta G°$ are listed in Table 4.

The relationship among the standard Gibb's free energy change ($\Delta G°$), enthalpy change ($\Delta H°$, J mol^{-1}), and entropy change ($\Delta S°$, J mol^{-1} K^{-1}) is expressed as Eq. (10).

$$\Delta G° = \Delta H° - T\Delta S° \tag{10}$$

Combining Eq. (9) with Eq. (10), Eq. (11) is obtained as follows.

$$\ln K_c = \frac{\Delta S°}{R} - \frac{\Delta H°}{RT} \tag{11}$$

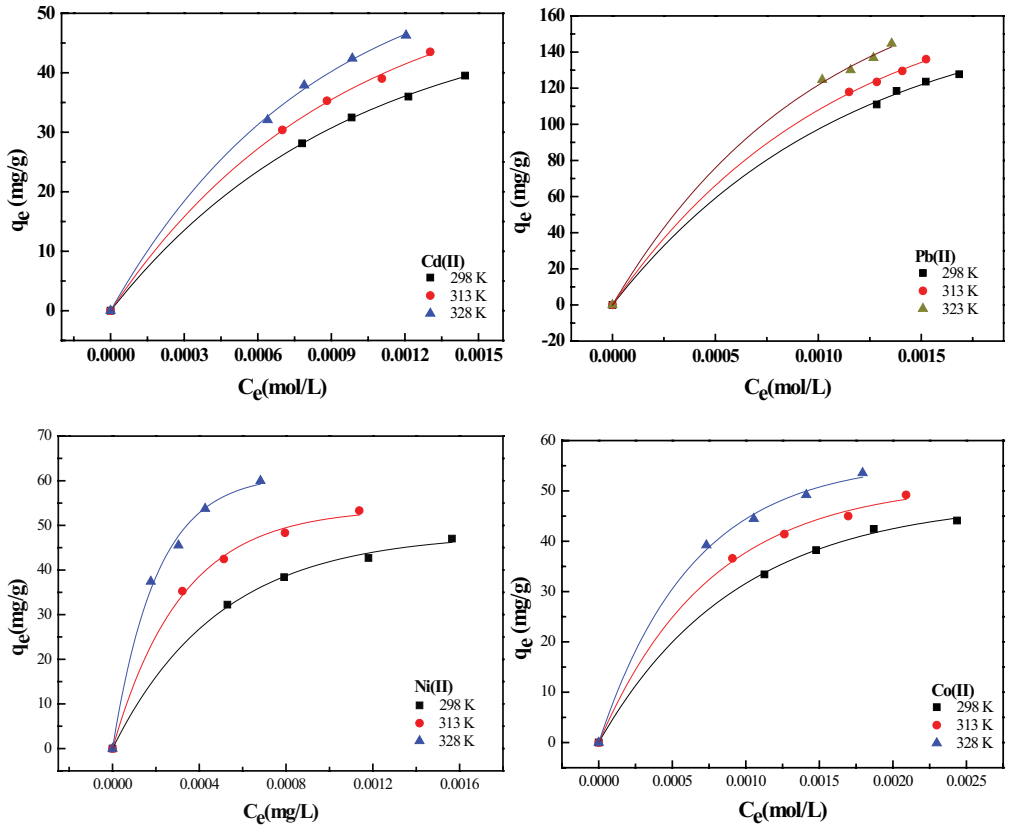

Fig. 10. Plots of q_e vs. C_e at different temperatures.

Table 4
Thermodynamic parameters for the adsorption of metallic cations on $CaTiO_3$ cuboid-like nanoparticles

Metallic cations	T (K)	K_c (L mol^{-1})	$\Delta G°$ (kJ mol^{-1})	$\Delta H°$ (kJ mol^{-1})	$\Delta S°$ (J k^{-1} mol^{-1})	R^2
Cd(II)	298	780	–16.5	3.2	66.0	0.8390
	313	806	–17.5			
	328	879	–18.5			
Pb(II)	298	704	–16.2	3.1	64.8	0.8308
	313	726	–17.2			
	328	790	–18.2			
Ni(II)	298	2,120	–19.0	23.9	144.0	0.9990
	313	3,424	–21.2			
	328	5,126	–23.3			
Co(II)	298	1,113	–17.4	9.7	1,165.6	0.9981
	313	1,329	–18.7			
	328	1,592	–20.1			

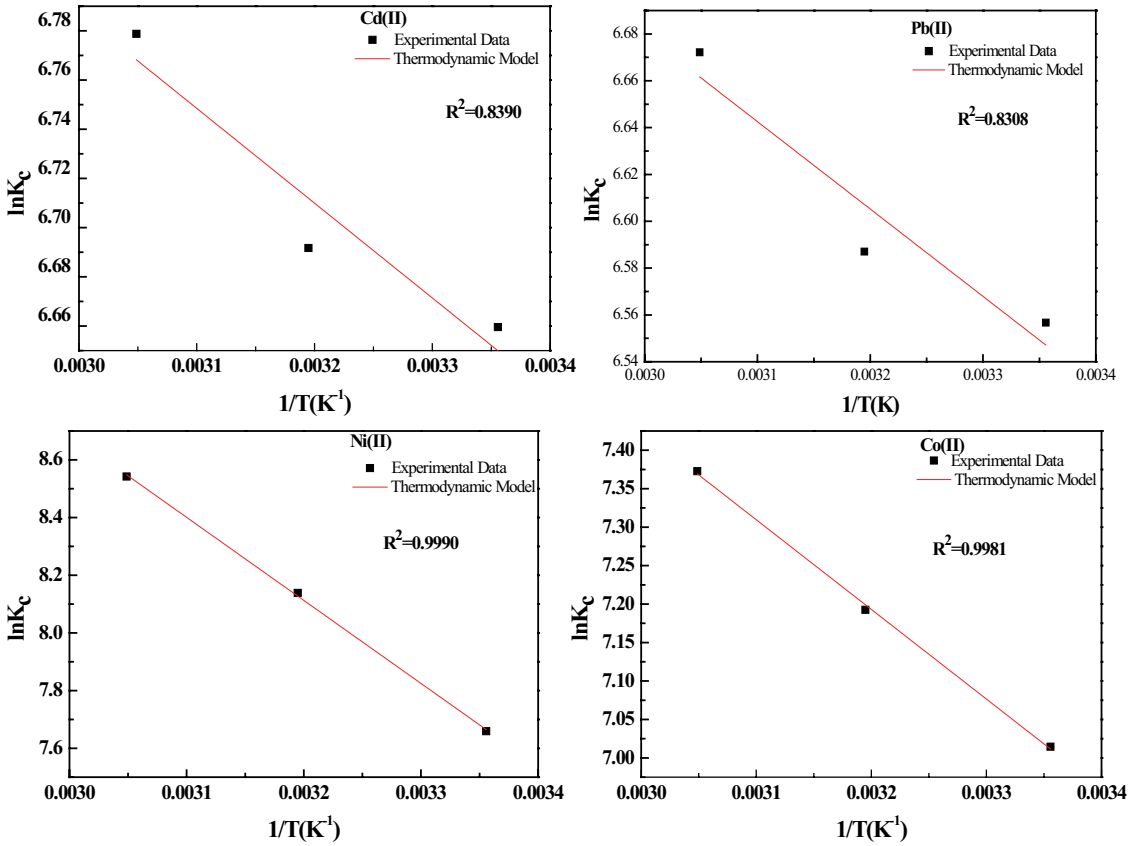

Fig. 11. Plots of lnK_c vs. 1/T for the adsorption of metallic cations on $CaTiO_3$ cuboid-like nanoparticles.

By plotting lnK_c vs. 1/T, a straight line could be obtained. The slope and intercept of the straight line are the values of -$\Delta H°/R$ and $\Delta S°/R$, respectively. And then the adsorption enthalpy change and entropy change can be calculated correspondingly.

The straight lines of lnK_c vs. 1/T for the adsorptions of Cd(II), Pb(II), Ni(II), and Co(II) cations on the $CaTiO_3$ cuboid-like nanoparticles are shown in Fig. 11. The thermodynamic parameters are listed in Table 4.

The adsorption thermodynamic analysis revealed that the values of $\Delta G°$ for the adsorption of Cd(II), Pb(II), Ni(II), and Co(II) cations on the $CaTiO_3$ nanoparticles were negative, indicating that the adsorption processes were spontaneous. The positive values of $\Delta H°$ indicated that the adsorption of these metallic cations was endothermic.

4. Conclusions

Calcium titanate ($CaTiO_3$) cuboid-like nanoparticles with the average widths and lengths of 101–184 nm and 203–329 nm were hydrothermally synthesized using metatitanic acid and calcium hydroxide as the raw materials at 120°C–180°C. The crystallization of $CaTiO_3$ nanoparticles was enhanced at higher reaction temperature and a longer reaction time period.

The as-synthesized $CaTiO_3$ cuboid-like nanoparticles exhibited higher adsorption capacities for the Cd(II), Pb(II), Ni(II), and Co(II) cations, which were higher than those over the reported porous $CaTiO_3$ synthesized by the solid-state reaction technique. The adsorption processes of these metallic cations on the $CaTiO_3$ cuboid-like nanoparticles were spontaneous and endothermic.

Acknowledgement

The present work was financially supported by the National Natural Science Foundation of China (21506078) and the Science and Technology Vice President Project of Jiangsu Province of China (FZ20180919).

References

[1] M. Sindhu, N. Ahlawat, S. Sanghi, A. Agarwal, R. Dahiya, N. Ahlawat, Rietveld refinement and impedance spectroscopy of calcium titanate, Curr. Appl. Phys., 12 (2012) 1429–1435.
[2] J.P. Singh, S. Gautam, P. Kumar, A. Tripathi, J.-M. Chen, K.H. Chae, K. Asokan, Correlation between the dielectric properties and local electronic structure of copper doped calcium titanate, J. Alloys Compd., 572 (2013) 84–89.
[3] J. Kotlana, P. Ctibor, Z. Pala, P. Homola, V. Nehasil, Improving dielectric properties of plasma sprayed calcium titanate ($CaTiO_3$) coatings by thermal annealing, Ceram. Int., 40 (2014) 13049–13055.
[4] L. Wang, J. Lia, M. Feng, L. Min, J. Yang, S. Yu, Y. Zhang, X. Hu, Z. Yang, Perovskite-type calcium titanate nanoparticles as novel matrix for designing sensitive electrochemical biosensing, Biosens. Bioelectron., 96 (2017) 220–226.
[5] N.Y. Yahya, N. Ngadi, M. Jusoh, N.A.A. Halim, Characterization and parametric study of mesoporous calcium titanate catalyst

for transesterification of waste cooking oil into biodiesel, Energy Convers. Manage., 129 (2016) 275–283.
[6] D. Zhang, S. Liu, X. Song, Z. Xu, B. Yang, L. Chen, Y. Tan, F. Li, Preparation of calcium titanate based on the cotton template method and its simultaneous removal performance to heavy metals and organic pollutants in water, J. Adv. Oxid. Technol., 19 (2016) 9–18.
[7] S.A. Hosseini, Preparation and characterization of calcium titanate nanoparticles with the aid of different acids and study of their photocatalytic properties, J. Mater. Sci. - Mater. Electron., 28 (2017) 3703–3708.
[8] J. Zhuang, Q. Tian, S. Lin, W. Yang, L. Chen, P. Liu, Precursor morphology-controlled formation of perovskites $CaTiO_3$ and their photo-activity for As(III) removal, Appl. Catal., B, 156–157 (2014) 108–115.
[9] H. Yoshida, L. Zhang, M. Sato, T. Morikawa, T. Kajino, T. Sekito, S. Matsumoto, H. Hirata, Calcium titanate photocatalyst prepared by a flux method for reduction of carbon dioxide with water, Catal. Today, 251 (2015) 132–139.
[10] G. Li, Q. Xiao, R. McNaughtond, L. Hane, L. Zhang, Y. Wang, Y. Yang, Nanoengineered porous chitosan/$CaTiO_3$ hybrid scaffolds for accelerating Schwann cells growth in peripheral nerve regeneration, Colloids Surf., B, 158 (2017) 57–67.
[11] Y. Tian, S. Fujibayashi, S. Yamaguchi, T. Matsushita, T. Kokubo, S. Matsuda, In vivo study of the early bone-bonding ability of Ti meshes formed with calcium titanate via chemical treatments, J. Mater. Sci. - Mater. Med., 26 (2015) 271.
[12] Z. Liu, K.C. Chan, L. Liu, S.F. Guo, Bioactive calcium titanate coatings on a Zr-based bulk metallic glass by laser cladding, Mater. Lett., 82 (2012) 67–70.
[13] S. Yamaguchi, T. Kizuki, H. Takadama, T. Matsushita, T. Nakamura,T. Kokubo, Formation of a bioactive calcium titanate layer on gum metal by chemical treatment, J. Mater. Sci. - Mater. Med., 23 (2012) 873–883.
[14] L.S. Cavalcante, V.S. Marques, J.C. Sczancoski, M.T. Escote, M.R. Joya, J.A. Varela, M.R.M.C. Santos, P.S. Pizani, E. Longo, Synthesis, structural refinement and optical behavior of $CaTiO_3$ Powders: a comparative study of processing in different furnaces, Chem. Eng. J., 143 (2008) 299–307.
[15] X. Lei, B. Xu, B. Yang, B. Xu, X. Guo, A novel method of synthesis and microstructural investigation of calcium titanate powders, J. Alloys Compd., 690 (2017) 916–922.
[16] S. Lanfredi, F. Storti, L.P.M. Simões, E. Djurado, M.A.L. Nobre, Synthesis and structural characterization of calcium titanate by spray pyrolysis method, Mater. Lett., 201 (2017) 148–151.
[17] S.K. Durrani, Y. Khan, N. Ahmde, M. Ahmad, M.A. Hussain, Hydrothermal growth of calcium titanate nanowires from titania, J. Iran. Chem. Soc., 8 (2011) 56–569.
[18] R.P. Schwarzenbach, B.I. Escher, K. Fenner, T.B. Hofstetter, C.A. Johnson, U. Gunten, B. Wehrli, The challenge of micropollutants in aquatic systems, Science, 313 (2006) 1072–1077.
[19] H. Bothe, A. Słomka, Divergent biology of facultative heavy metal plants, J. Plant Physiol., 219 (2017) 45–61.
[20] J. Cho, S. Hyun, J.-H. Han, S. Kim, D.-H. Shin, Historical trend in heavy metal pollution in core sediments from the Masan Bay, Korea, Mar. Pollut. Bull., 95 (2015) 427–432.
[21] U.K. Garg, M.P. Kaur, V.K. Garg, D. Sud, Removal of hexavalent chromium from aqueous solution by agricultural waste biomass, J. Hazard. Mater., 140 (2007) 60–68.
[22] Y. Chen, X. Jiang, Y. Wang, D. Zhuang, Spatial characteristics of heavy metal pollution and the potential ecological risk of a typical mining area: a case study in China, Process Saf. Environ. Prot., 113 (2018) 204–219.
[23] H.S. Altundogan, Cr(VI) removal from aqueous solution by iron (III) hydroxide-loaded sugar beet pulp, Process Biochem., 40 (2005) 1443–1452.
[24] V. Manirethan, K. Raval, R. Rajan, H. Thaira, R.M. Balakrishnan, Kinetic and thermodynamic studies on the adsorption of heavy metals from aqueous solution by melanin nanopigment obtained from marine source: *Pseudomonas stutzeri*, J. Environ. Manage., 214 (2018) 315–324.
[25] D. Kołodynska, J. Krukowska-Bąk, J. Kazmierczak-Razna, R. Pietrzak, Uptake of heavy metal ions from aqueous solutions by sorbents obtained from the spent ion exchange resins, Microporous Mesoporous Mater., 244 (2017) 127–136.
[26] M. Wu, J. Liang, J. Tang, G. Li, S. Shan, Z. Guo, L. Deng, Decontamination of multiple heavy metals-containing effluents through microbial biotechnology, J. Hazard. Mater., 337 (2017) 189–197.
[27] O. Tavakoli, V. Goodarzi, M.R. Saebc, N.M. Mahmoodi, R. Borja, Competitive removal of heavy metal ions from squid oil under isothermal condition by CR11 chelate ion exchanger, J. Hazard. Mater., 334 (2017) 256–266.
[28] W. Yao, J. Wang, P. Wang, X. Wang, S. Yu, Y. Zou, J. Hou, T. Hayat, A. Alsaedi, X. Wang, Synergistic coagulation of GO and secondary adsorption of heavy metal ions on Ca/Al layered double hydroxides, Environ. Pollut., 229 (2017) 827–836.
[29] Y. Li, D. Zhang, Application of porous nano-calcium titanate in preconcentration of heavy metals in water, Am. Lab., 46 (2014) 32–35.
[30] D. Zhang, P. Yu, X. He, Preparation and characterization of porous calcium titanate-based coated glass fiber filter material and its application in determination of lead and cadmium ion concentrations in water, J. AOAC Int., 94 (2011) 1925–1933.
[31] D. Zhang, C. Zhan, P. Zhou, Preparation of porous nano-calcium titanate microspheres and its adsorption behavior for heavy metal ion in water, J. Hazard. Mater., 186 (2011) 971–977.
[32] M. Foroughi-dahr, H. Abolghasemi, M. Esmaili, A. Shojamoradi, H. Fatoorehchi, Adsorption characteristics of Congo red from aqueous solution onto tea waste, Chem. Eng. Commun., 202 (2015) 181–193.
[33] Y. Hang, H. Yin, Y. Ji, Y. Liu, Z. Lu, A. Wang, L. Shen, H.X. Yin, Adsorption performances of naked and 3-aminopropyl triethoxysilane-modified mesoporous TiO_2 hollow nanospheres for Cu^{2+}, Cd^{2+}, Pb^{2+}, and Cr(VI) ions, J. Nanosci. Nanotechnol., 17 (2017) 5539–5549.
[34] T. Fan, Y. Liu, B. Feng, G. Zeng, C. Yang, M. Zhou, H. Zhou, Z. Tan, X. Wang, Biosorption of cadmium(II), zinc(II) and lead(II) by *Penicillium simplicissimum*: isotherms, kinetics, and thermodynamics, J. Hazard. Mater., 160 (2008) 655–661.
[35] Ş. Yılmaz, Ü. Ecer, T. Şahan, Modelling and optimization of As(III) adsorption onto thiol-functionalized bentonite from aqueous solutions using response surface methodology approach, Chemistry Select, 3 (2018) 9326–9335.
[36] Ü. Ecer, Ş. Yılmaz, T. Şahan, Highly efficient Cd(II) adsorption using mercapto-modified bentonite as a novel adsorbent: an experimental design application based on response surface methodology for optimization, Water Sci. Technol., 78 (2018) 1348–1360.
[37] Y. Liu, Is the free energy change of adsorption correctly calculated?, J. Chem. Eng. Data, 54 (2009) 1981–1985.
[38] Y. Liu, Y.-J. Liu, Biosorption isotherms, kinetics and thermodynamics, Sep. Purif. Technol., 61 (2008) 229–242.
[39] Y. Liu, H. Xu, Equilibrium, thermodynamics and mechanisms of Ni^{2+} biosorption by aerobic granules, Biochem. Eng. J., 35 (2007) 174–182.